Bioinspiration & Biomimetics

PAPER

The influence of substrate roughness, patterning, curvature, and compliance in peeling problems

Lucas Brely[1], Federico Bosia[1] and Nicola M Pugno[2,3,4]

[1] Department of Physics and 'Nanostructured Interfaces and Surfaces' Inter-Departmental Centre, Università di Torino, Via P. Giuria 1, 10125, Torino, Italy
[2] Laboratory of Bio-Inspired and Graphene Nanomechanics, Department of Civil, Environmental and Mechanical Engineering, Università di Trento, via Mesiano, 77, I-38123 Trento, Italy
[3] School of Engineering and Materials Science, Queen Mary University of London, Mile End Road, London E1 4NS, United Kingdom
[4] Ket Lab, Edoardo Amaldi Foundation, Italian Space Agency, Via del Politecnico snc, 00133 Rome, Italy

E-mail: nicola.pugno@unitn.it

RECEIVED
5 August 2017

REVISED
30 November 2017

ACCEPTED FOR PUBLICATION
12 December 2017

PUBLISHED
19 January 2018

Keywords: adhesion, substrate properties, numerical simulation

Abstract

Biological adhesion, in particular the mechanisms by which animals and plants 'stick' to surfaces, has been widely studied in recent years, and some of the structural principles have been successfully applied to bioinspired adhesives. However, modelling of adhesion, such as in single or multiple peeling theories, has in most cases been limited to ideal cases, and due consideration of the role of substrate geometry and mechanical properties has been limited. In this paper, we propose a numerical model to evaluate these effects, including substrate roughness, patterning, curvature, and deformability. The approach is validated by comparing its predictions with classical thin film peeling theoretical results, and is then used to predict the effects of substrate properties. These results can provide deeper insight into experiments, and the developed model can be a useful tool to design and optimize artificial adhesives with tailor-made characteristics.

1. Introduction

In recent years, there has been growing interest in the study of biological systems displaying architectures that are optimized for specific functions such as structural resilience, protection, locomotion, self-cleaning, or self-repair [1–3]. The observation and mimicry of natural systems has therefore led to the emergence of novel smart strategies to improve artificial system functionalities [4]. This applies to the field of biological adhesion, which also studies the way in which animals like beetles, spiders, or geckos achieve optimized adhesion control by arrays of tape-like micro- or nano-contacts organized in a hierarchical manner, especially in heavier animals [5]. It has been demonstrated that these contact units can be modelled as delaminating (or 'peeling') thin films, rather than punch-like units [6], and that structures such as gecko, spider, or insect pads can be described using models based on this description of the contacts [7, 8]. One of the key features of analytical tape peeling models, such as the Rivlin model [9] or the Kendall model [10], is that the peeling force, i.e. the force necessary to initiate detachment of the adhesive structure, strongly depends on the angle between the applied force and the substrate, i.e. the 'peeling angle'. In addition to the observed contact geometries, one of the main arguments for treating animal attachment as ensembles of delaminating tapes is that the angle dependence on the detachment force has been experimentally observed in all species displaying 'hairy' contacts, both at micro and macro scales [5]. In addition to the geometry of the tape unit and the peeling angle, the adhesive energy at the interface between the contact units and the substrate contributes to determining the peeling force. This adhesive energy is mainly due to van der Waals interactions [11] and to capillarity [12], but in the cited contact models all substrate and interface properties are condensed into a single adhesive energy term. For a given loading scenario and tape geometrical/mechanical properties, the adhesive energy varies as a function of the material and the surface profile of the substrate [13, 14]. In turn, the peeling force derived in analytical peeling models is related to the variation of the difference between adhesive energy and total potential energy, which describes the micro scale physics of interface failure.

With current progress in mimicking natural adhesives, the understanding of peeling mechanisms and the derivation of adhesion optimization criteria

become essential. To design optimal solutions, adequate numerical tools taking account of all mechanical mechanisms are required, and thus reliable models need to be developed. One of the main drawbacks of current models and of Kendall's formulation in particular, is that they do not account for the dependence of the adhesive force on substrate properties, i.e. the substrate is considered perfectly flat and infinitely rigid. However, outstanding adhesive properties of animal attachment systems also appear in the presence of variable substrate compliance, roughness, or of structured surfaces [15]. These essential features should therefore also be included in models, especially in the case of soft substrate materials.

Persson *et al* [16, 17] presented a theoretical study on the influence of surface roughness occurring at various size scales on the adhesive properties of biological adhesives, showing that a hierarchical fibrillar structure is essential in guaranteeing sufficient adaptability to the surface. Peng *et al* proposed an analytical model to describe the effect of roughness on an elastic nanofilm, linking its adhesion to the 'wavelength' of the roughness profile [18]. Huber *et al* [19] and Cañas *et al* [20] presented experimental studies on the effect of surface roughness on artificial adhesives with spatula- or mushroom-shaped tips, including qualitative analysis of the assumed mechanisms for adhesion enhancement for varying asperity size scales. The issue of roughness as a cause for partial contact was addressed in [21], where the Johnson, Kendall, and Roberts (JKR) theory was extended to account for energy released during rippling. A review of these and other modelling approaches related to the influence of roughness is provided in [22]. However, in these works, the effect of roughness or surface patterning on adhesive strength is not explicitly correlated to the dimension of the process zone, i.e. the size scale at which stress concentrations occur in peeling processes.

In this paper, we adopt a different approach to address the issue of surface roughness and patterning, adding analysis of the influence of substrate curvature and compliance, with the objective of better understanding the role of the substrate on the peeling behaviour of adhesives. We present a novel computational approach to model the so-called process zone of peeling, which is the area where the interface between the adhesive and substrate is subject to stresses, leading to failure of adhesive bonds and therefore to detachment. The model is validated with results from classical peeling theories, and several aspects of the interface/substrate are discussed.

2. Analytical modelling of the process zone

We consider a problem of dry adhesion of a contact unit on a substrate. The mechanics of its detachment, illustrated in figure 1(A), is analogous to the problem of a propagating crack front in an adhesive interface. A classical energetic approach such as Kendall's model [10] provides a macro scale description of this mechanism, and is the reference model in the study of biological adhesion. The progression of the peeling front becomes energetically favourable, and therefore occurs if

$$\frac{\partial V}{\partial l_\mathrm{d}} - \frac{\partial U_\mathrm{e}}{\partial l_\mathrm{d}} > \frac{\partial U_\mathrm{s}}{\partial l_\mathrm{d}}, \tag{1}$$

where V is the work associated with the external load applied to the tape, U_e is the stored elastic energy in the tape, U_s is the surface energy, and l_d is the detached tape length, which increases as the peeling proceeds. When delamination occurs, the dissipated energy per unit detached surface area, indicated in linear elastic fracture mechanics as the strain energy release rate [23], equals the adhesive energy G per unit area of the interface:

$$G = \frac{1}{w}\left(\frac{\partial U_\mathrm{s}}{\partial l_\mathrm{d}}\right), \tag{2}$$

where w is the tape width. According to Kendall's theory, this corresponds to

$$G = \frac{1}{w}\left(\frac{\partial V}{\partial l_\mathrm{d}} - \frac{\partial U_\mathrm{e}}{\partial l_\mathrm{d}}\right) = \frac{F}{w}(1-\cos\theta) + \frac{F^2}{2Ebw^2}, \tag{3}$$

where F is the applied load at the detached tape end, b is the tape thickness, E is the tape elastic modulus, and θ is the angle between the applied load and the substrate (figure 1(A)). The critical peeling force F_c therefore becomes

$$F_\mathrm{c} = Ebw\left(\cos\theta - 1 + \sqrt{(1-\cos\theta)^2 + \frac{2G_\mathrm{c}}{Eb}}\right). \tag{4}$$

Another approach in the study of adhesion and delamination is to determine the loading state of the interface, assuming a thin adhesive layer bonding the tape and the substrate [24]. In this formulation, a finite-length region exists in the vicinity of the propagating delamination front, referred to as the process zone, in which deformations in both the tape and the interface take place [25]. Considering a simple loading scenario where the applied external load is parallel to the substrate at $\theta = 0$, the force balance acting on the attached region, according to the shear lag model [26], can be written as

$$\frac{\mathrm{d}\sigma_\mathrm{T}}{\mathrm{d}x} = \frac{\tau_\mathrm{I}}{b}, \tag{5}$$

where $\mathrm{d}\sigma_\mathrm{T}$ is the infinitesimal variation of the tape axial stress over an infinitesimal length $\mathrm{d}x$, and τ_I is the shear stress in the interface layer, which is assumed initially to be a linear function of the axial displacement u within the tape and the interfacial stiffness K_I in the tangential direction:

$$\tau_\mathrm{I} = K_\mathrm{I} u. \tag{6}$$

Introducing the tape strain $\epsilon_\mathrm{T} = \mathrm{d}u/\mathrm{d}x = \sigma_\mathrm{T}/E$, after differentiation of equation (5), we obtain

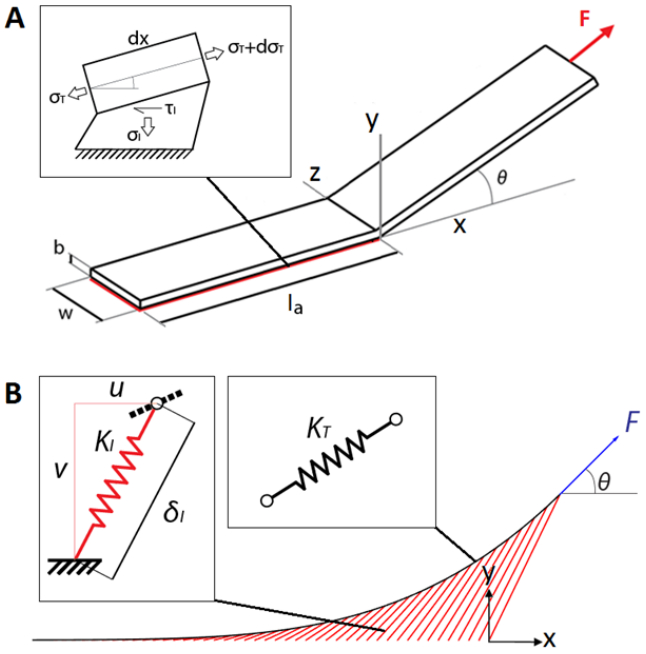

Figure 1. (A) Schematic representation of the geometry of the considered tape peeling problem and (inset) of the stresses acting on an elementary unit of the interface. (B) Corresponding discretization in the numerical model using interface and tape spring elements of stiffnesses K_I and K_T, respectively.

$$\frac{d^2\sigma_T}{dx^2} = \frac{K_I}{bE}\sigma_T. \tag{7}$$

This equation is solved by applying the boundary conditions $\sigma_T(x=0) = F/(bw)$, and supposing that the attached length l_a of the tape is sufficiently long for the tape axial stress to tend to zero at its edge $\sigma_T(x \to -l_a) = 0$. In this case, we obtain the following distribution of interfacial stress:

$$\tau_I(x) = \frac{F}{w}\sqrt{\frac{K_I}{bE}}\exp\left(\sqrt{\frac{K_I}{bE}}x\right). \tag{8}$$

In correspondence with the peeling line at $x = 0$, the interfacial stress is maximum, and failure of the adhesive bond occurs when its elastic energy reaches the critical value:

$$G_c = \frac{F_c^2}{2Ebw^2} = \frac{\tau_{Ic}^2(x=0)}{2K_I}. \tag{9}$$

This equation also provides the relation between interface stress distribution and the detachment force. The critical peeling force (9) is in agreement with Kendall's equation (4) for $\theta = 0$, showing the consistency of the approach with existing peeling theories. Notice that previous works have investigated the influence of bending stiffness on the peeling behaviour of thin films [27]. In the present paper, we consider the bending stiffness to be negligible, and tape thickness values will be chosen accordingly.

When the peeling angle differs from zero, the adhesive bonds experience both tangential and normal loads, whose distributions influence the external force at which the system detaches. The interface is therefore subject to a mixed-mode fracture mechanism with an opening mode (mode-I) and a sliding mode (mode-II). For small peeling angles, the mode-II strain energy release rate G_{II} can be approximated by solving equation (7) with the boundary condition $F(x=0) = F\cos\theta$, leading to

$$G_{II} = \frac{F^2}{2Ebw^2}\cos^2\theta. \tag{10}$$

The mode-I strain energy release is estimated by injecting equation (10) into (3) with $G = G_I + G_{II}$, leading to

$$G_I = \frac{F^2}{2Ebw^2}\sin^2\theta + \frac{F}{w}(1-\cos\theta). \tag{11}$$

3. Numerical model and results

We now propose a numerical model to determine both tangential and normal stress distributions at the interface, and to understand how the mechanisms acting within the process zone affect the overall adhesive performance. The tape is thus discretized with a set of truss members of length Δx (the discretization length), undergoing axial load only. A traction versus separation law, usually referred to as a cohesive zone model [28], is introduced for each tape node to model the interface between the tape and the substrate, i.e. a restoring reaction force is generated on the tape nodes as a function of the deformations of the system. The relation between the tape axial stress and strain is taken as linear elastic for simplicity, but geometrical nonlinearities can occur in interfacial stresses due to the nature of the problem. As the

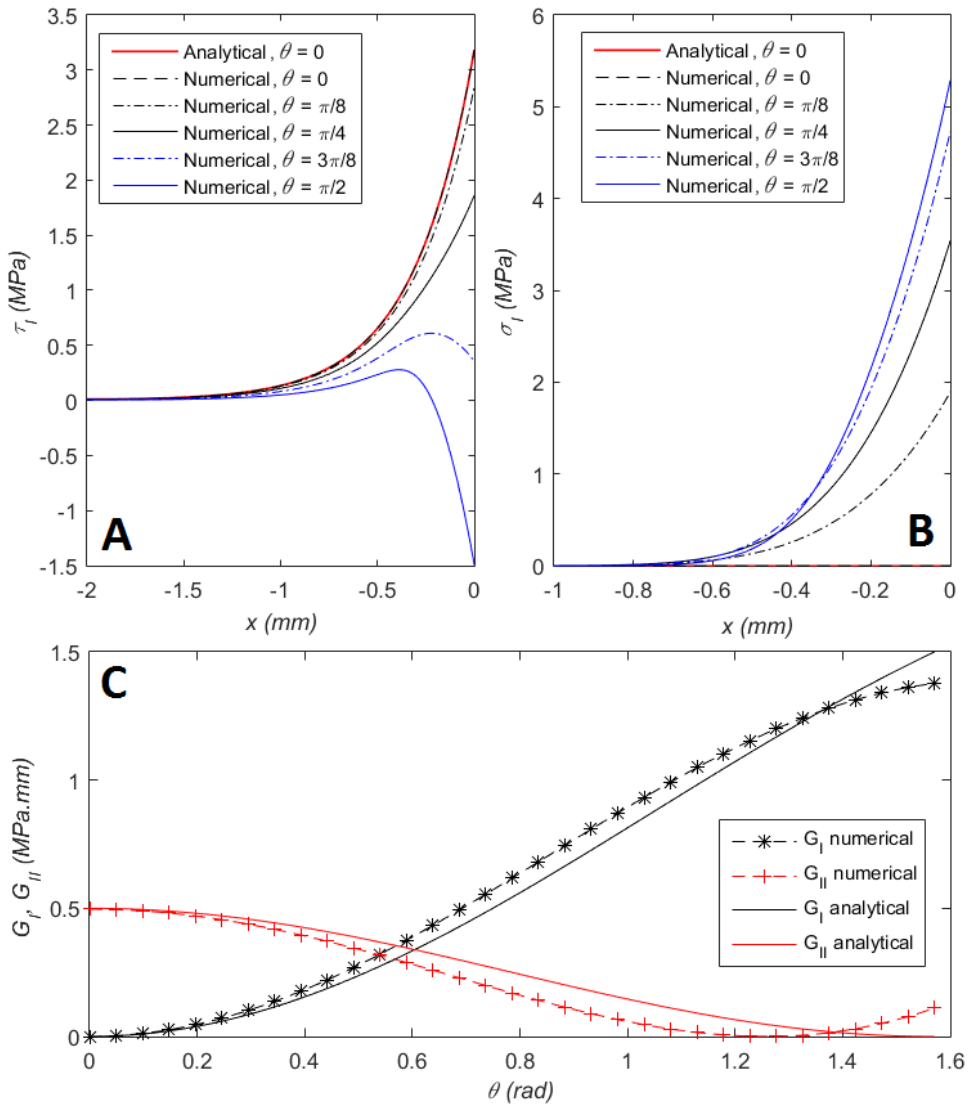

Figure 2. (A) Shear and (B) normal stress distributions at the interface along the process zone for different peeling angles. (C) Mode-I and mode-II strain energy release rate as a function of the peeling angle.

applied force and its angle with respect to the substrate increase, deformations, translations, and rotations of the tape vary in the process zone, as does the stored elastic energy of the adhesive interface bonds, which are responsible for the macroscopic behaviour of the peeling system. To calculate the mechanical equilibrium after the application of the force, a Newton–Raphson iterative scheme [29] is adopted (details are given in the appendix). A 2D model is employed, assuming that the detached and attached tape regions and the applied force are coplanar. The detached part of the tape is not modelled, since the far-field external load can be directly applied in correspondence with the peeling line at $x = 0$. This is because the tape bending stiffness is neglected so that the detached part of the tape only transfers axial load without influencing the mechanical equilibrium of the process zone. We introduce a linear interfacial traction versus separation law as

$$\frac{R}{w\Delta x} = K_{\mathrm{I}}\delta_{\mathrm{I}}, \tag{12}$$

where R is the nodal reaction force, and $\delta_{\mathrm{I}} = \sqrt{u^2 + v^2}$ is the separation of a tape node with respect to its initial position in the plane, with u and v being the components of the nodal displacement along x and y. Notice that interface bonds experience axial load only (tangential and normal forces are coupled). A schematization of the numerical model is shown in figure 1(B).

In the following, tape and interface properties are chosen as $w = 1\,\mathrm{mm}$, $b = 0.01\,\mathrm{mm}$, $K_{\mathrm{I}} = 10\ \mathrm{MPa}\cdot\mathrm{mm}^{-1}$, $l_{\mathrm{a}} = 2\,\mathrm{mm}$, and an external load of $F = 10\,\mathrm{N}$ is applied. The tape Young's modulus is chosen as $E = 100\,\mathrm{MPa}$ because although biological fibrillar adhesives reach values above 1 GPa [17, 22, 30], recent studies indicate that the modulus decreases towards the tips of the contacts [31]. The corresponding tangential and normal stress distributions, calculated from the displacement field at equilibrium as $\tau_{\mathrm{I}} = K_{\mathrm{I}}u$ and $\sigma_{\mathrm{I}} = K_{\mathrm{I}}v$, as a function of the peeling angle are shown in figures 2(A) and (B). These distributions highlight the fact that the angle dependency is

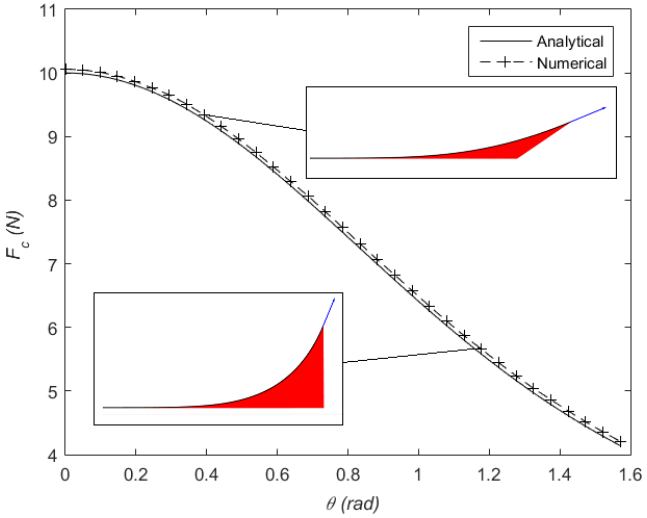

Figure 3. Peeling force versus peeling angle with the present numerical model and the theoretical result. Inset: interface deformation states at two different peeling angles.

related to stress distributions within the process zone. At $\theta = 0$, the normal stress is zero, and the shear stress distribution agrees with the analytical solution in equation (8) (shown in red). We note that the normal interfacial stress is more concentrated at the peeling line compared to the shear one, and is mainly responsible for the decrease in the peeling force as the peeling angle is increased. In addition, no compressive normal stress is present ahead of the peeling front, which is consistent with the fact that with the chosen parameters the bending stiffness is negligible.

In the numerical model, the mode-I and mode-II strain energy release rates are computed from the displacement field at the most critical adhesive bond (in correspondence with the peeling line) as follows:

$$G_{\mathrm{I}} = \frac{1}{2} K_{\mathrm{I}} v^2, \tag{13}$$

$$G_{\mathrm{II}} = \frac{1}{2} K_{\mathrm{I}} u^2. \tag{14}$$

The dependence of G_{I} and G_{II} on the peeling angle θ, calculated both analytically and numerically, is shown in figure 2(C). There is a good agreement between analytical and numerical results, but for large peeling angles, rigid body motions of the tape and large adhesive bond deformations within the process zone affect the interfacial stress distribution and lead to a discrepancy between the two.

We now introduce a local energy-based failure criterion, i.e. a critical strain energy release rate G_{c} for the interface bonds, beyond which detachment occurs as

$$G_{\mathrm{c}} = \frac{1}{2} K_{\mathrm{I}} \delta_{\mathrm{I}}^2. \tag{15}$$

The corresponding peeling force as a function of the peeling angle calculated numerically agrees with the analytical solution of equation (3), as shown in figure 3 for an adhesive energy $G_{\mathrm{c}} = 0.5$ MPa·mm.

In nature, a wide variety of types of bonding between the tape-like contacts and the substrate has been observed in biological systems. The van der Waals interaction responsible for the adhesion of geckos, the capillarity forces in insect attachment or glue-coated spider silks all have specific interactions with the substrate. The traction–separation law is therefore expected to depend on the type of interaction. In the case of a nonlinear force versus separation relation of the interface bonds, the peeling force is not affected by the type of nonlinearity as long as the total energy dissipated by a specific bond during loading is invariant. This means that although the model has been developed for dry adhesion, wet adhesion can also be simulated, provided an appropriate adhesive term can be formulated. We thus consider different traction–separation laws (reaction force R versus elongation δ_{I}) in the model:

- Linear elastic:

$$\frac{R}{w\Delta x} = \begin{cases} K_{\mathrm{I}}\delta_{\mathrm{I}} & \text{for } \delta_{\mathrm{I}} < \delta_{\mathrm{I}}^* \\ 0 & \text{for } \delta_{\mathrm{I}} > \delta_{\mathrm{I}}^* \end{cases}. \tag{16}$$

- Perfectly elastoplastic:

$$\frac{R}{w\Delta x} = \begin{cases} K_{\mathrm{I}}\delta_{\mathrm{I}} & \text{for } \delta_{\mathrm{I}} < \delta_{\mathrm{I}}^* \\ K_I\ \delta_{\mathrm{I}}^* & \text{for } \delta_{\mathrm{I}} > \delta_{\mathrm{I}}^* \\ 0 & \text{for } \delta_{\mathrm{I}} > \delta_{\mathrm{I}}^{**} \end{cases}. \tag{17}$$

- Exponential:

$$\frac{R}{w\Delta x} = \frac{R^*}{w\Delta x}\frac{\delta_I}{\delta_{\mathrm{I}}^*}\exp\left(1 - \frac{\delta_{\mathrm{I}}}{\delta_{\mathrm{I}}^*}\right). \tag{18}$$

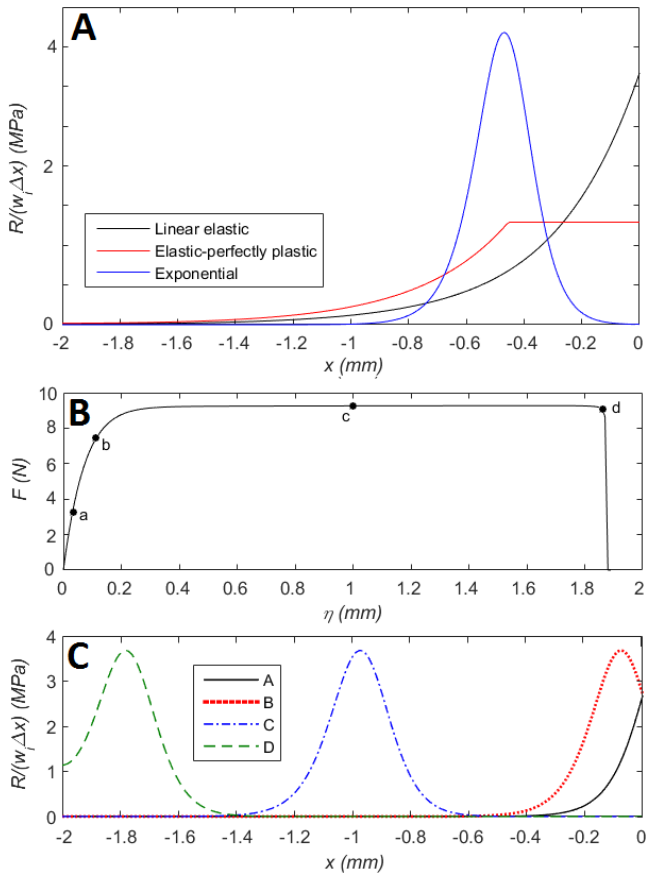

Figure 4. (A) Interface bond axial stress along the process zone for different traction–separation laws when the peeling force is reached (for $\theta = \pi/8$). (B) Resulting force–displacement relationship in the peeling test for an exponential traction–separation law. (C) Propagation of the peeling front corresponding to points (a)–(d), visualized using the interface bond axial stress distribution.

The input parameters for each of these laws must satisfy the following condition:

$$\int_0^\infty \frac{R}{w\Delta x} \mathrm{d}\delta_I = G_\mathrm{c}. \tag{19}$$

When the peeling force is reached, the load distribution at the interface $\frac{R}{w\Delta x}$ versus x changes considerably as a function of the chosen traction–separation law, as shown in figure 4(A) (for $\theta = \pi/8$ and $G_\mathrm{c} = 0.5$ MPa·mm).

The applied force versus force application point displacement η obtained for a peeling test, i.e. when the system is loaded until complete detachment of the tape, is shown in figure 4(B) for an exponential traction–separation law and $\theta = \pi/8$, highlighting an 'elastoplastic' behaviour. When the applied load is below the peeling force (points (a) and (b)), the elastic energy in the interface increases as it deforms. Next, the crack front propagates at a constant peeling force (point (c)) over the attached length of the tape. A small drop in the peeling force is observed (point (d)) when the crack front reaches the end of the attached region, before complete detachment. This is because the remaining attached part is not long enough for the axial load in the tape, and consequently the interface load, to tend to zero (figure 4(C)).

4. Influence of substrate geometrical features

We now study the influence of several characteristics of the substrate on the peeling force using the previously introduced numerical model. For simplicity, the linear traction–separation law is employed for the interface in simulations, together with the local energy-based delamination criterion.

4.1. Substrate roughness and patterning

An imperfect contact between the tape and the substrate, as a result of surface roughness, can be introduced by statistically assigning a variable adhesive energy G_c^* to each adhesive bond. These energy values are extracted randomly from a uniform distribution $G_\mathrm{c}^* = 2 \cdot U(0, G_\mathrm{c})$, and from a normal distribution $G_\mathrm{c}^* = \mathcal{N}(G_\mathrm{c}, G_\mathrm{c}/10)$ with $G_\mathrm{c} = 1$ MPa.mm. The first of the two is considered since it allows us to evaluate the effect of a large scatter in adhesive energy values. The second of the two is closer to the surface roughness distribution found in real materials. The simulation is performed for $\theta = 0$ and $\theta = \pi/4$. The corresponding force–displacement plot of the force application point η is shown in figure 5(A). The general behaviour of the system is similar to that for a smooth substrate shown

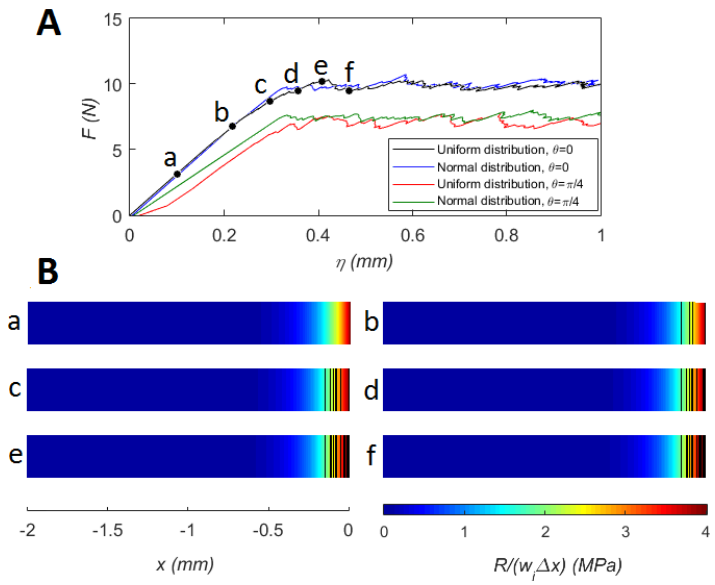

Figure 5. (A) Force F versus displacement η during peeling of a tape from a substrate with nonzero surface roughness for two different peeling angles and roughness distributions (compare to figure 4(B) for a smooth surface). (B) Corresponding propagation of the peeling front in the early stages of detachment at points a to f along the F versus η curve. The colour scale represents the interfacial load distributions. The areas where local detachments occur are represented in black.

in figure 4(B). The two plots refer to different traction–separation laws, but this does not influence the overall behaviour, provided the integral in equation (19) is the same. The peeling force appears to be approximately constant in spite of the high variability in the local failure energies. It is interesting to note that the obtained peeling forces are $F_c(\theta = 0) \cong 10\,\mathrm{N}$ and $F_c(\theta = \pi/4) \cong 7.41\,\mathrm{N}$, which are approximately those predicted by equation (4) considering the mean value $G_c = 0.5\,\mathrm{MPa} \cdot \mathrm{mm}$. The time variation of the load distribution is shown in figure 5(B) in the case of a uniform distribution at $\theta = 0$, and helps us gain a better understanding of the peeling force results. In the early stages of loading of the system, some local detachment events occur ahead of the crack front, in correspondence with the weakest adhesive bonds, and the load is then distributed on the surviving ones, driving the peeling force.

Another important effect related to the substrate morphological properties is the possible presence of entire regions where contact is absent, such as in the case of patterned surfaces. To investigate this, we simulated numerically the case of a periodic pattern schematically shown in figure 6(A), by alternating regions without and with bonding between the tape and the substrate, of lengths α and β, respectively. The results of the simulations for $\theta = \pi/8$ and varying α and β values are shown in figure 6(B). Here, the maximum peeling force for the considered structure is normalized with respect to the one predicted by equation (4), i.e. for full contact over the entire substrate. When the length of the attached region β reaches the theoretical process zone length, the normalized force tends to 1, which means that the pattern does not affect the process zone distribution. As β decreases, the maximum peeling force is reduced due to an increase in the load concentration within the process zone. The size of the gaps within the attached region also affects the peeling force. As the length α increases, the detachment force decreases for a fixed β. Simulations show that patterned substrate surfaces are detrimental to the peeling force, especially when the size of gaps in the interface is large with respect to the process zone length. Figure 6(C) shows that the peeling force is not constant during a peeling test on a patterned substrate. As the first attached length ahead from the peeling front is reduced, the peeling force tends to decrease until the detachment front encounters a detached region. Then, the force increases again as the crack is stopped and the tape undergoes elastic deformation until the next attached length starts to peel off. The difference between the minimum and maximum detachment force in this case increases as the unbounded lengths α are increased.

4.2. Substrate curvature

In [14], the ability of the gecko's lamellar system to adapt to wavy surfaces was studied. Specifically, the influence of substrates characterized by a sinusoidal profile on the shear adhesion strength was considered. Depending on the amplitude and wavelength of the considered surface profile, the hierarchical adhesive pad of the gecko has full or partial contact with the substrate. When partial contact is achieved, the problem is similar to that discussed in the previous section, but when tape-like structures of lamellae conform to the curvature of the surface, the process zone load distribution differs from the flat surface case. A radius of curvature for convex and concave surfaces can be simply introduced in the present model

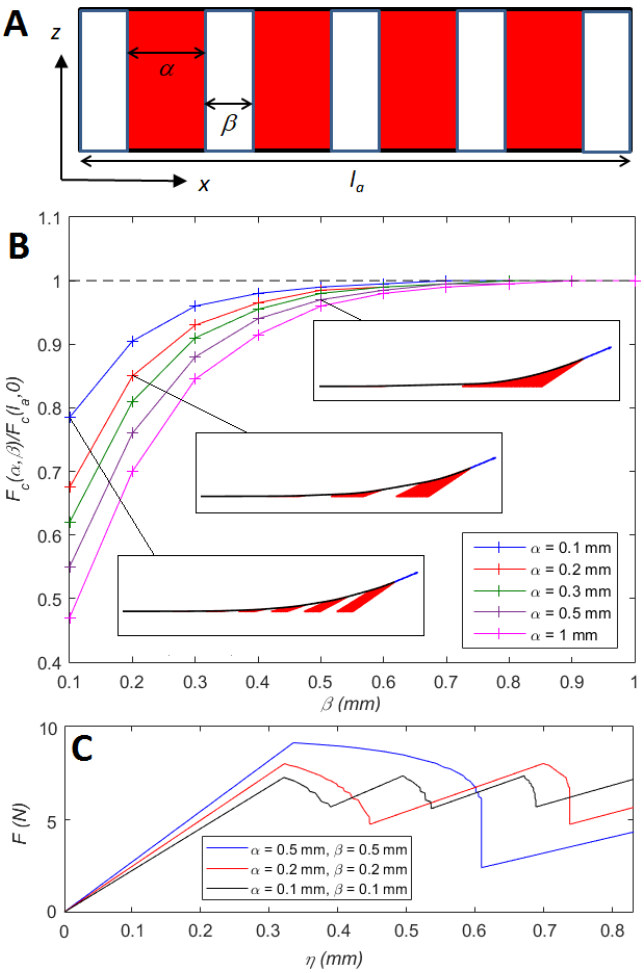

Figure 6. (A) Schematic of the periodic patterned surface with alternating non-contacting lengths α and lengths in contact β. (B) Normalized peeling force versus β for various α values. Inset: corresponding deformation states. (C) Corresponding force F versus displacement η during peeling test.

by setting the initial coordinates of the tape nodes along an arc of a circle rather than a line. The peeling angle in this case is the angle between the applied external load and the tangent to the substrate surface at the peeling line, and the adhesive energy is set to constant on all points of the model. When the length of the process zone is small with respect to the radius of curvature of the surface (in our case approximately 1 mm), this effect is negligible; however, as it decreases and becomes of comparable size, the peeling force is affected. Figure 7 shows the peeling force, normalized with respect to the peeling force on a flat substrate with the same parameters, as a function of the radius of curvature. For convex surfaces, the peeling force increases as the curvature radius decreases, and the opposite happens for concave surfaces. Additionally, the peeling angle changes as the detachment proceeds and the peeling force is not constant during propagation of the peeling front, which is contrary to the case for a flat surface. This is illustrated in figure 7(C), where the force tends to increase for convex surfaces, and decrease for concave surfaces. When the contacts are split, the adhesive strength is the result of simultaneous delamination of multiple tapes [25], as is the case for animal hairy attachments, and the decrease in local angles at different hierarchical scales could help in optimizing the total peeling force.

5. Influence of substrate deformation

In the case of soft materials, substrate deformation can also affect the way the load is distributed in peeling tests. The inclusion of substrate deformation in the calculation of the peeling force is a complex problem, since implementing an elastic half-plane in the simulation with a sufficient precision, i.e. a sufficiently small discretization length, would lead to a very large number of degrees of freedom. Instead, we propose to introduce an elastic foundation of stiffness K_S in both normal and tangential directions for the substrate nodes. The interface is therefore introduced in the numerical model as a set of interface and substrate bonds arranged in series. The local failure criterion is still applied to the interface bonds when the system is loaded, in the hypothesis that no failure events take place within the substrate. Figure 8 shows, for a uniform adhesive energy, the peeling force as a function of the ratio between the interface and the substrate stiffness. A more compliant substrate generates a higher peeling force, which tends to the theoretical

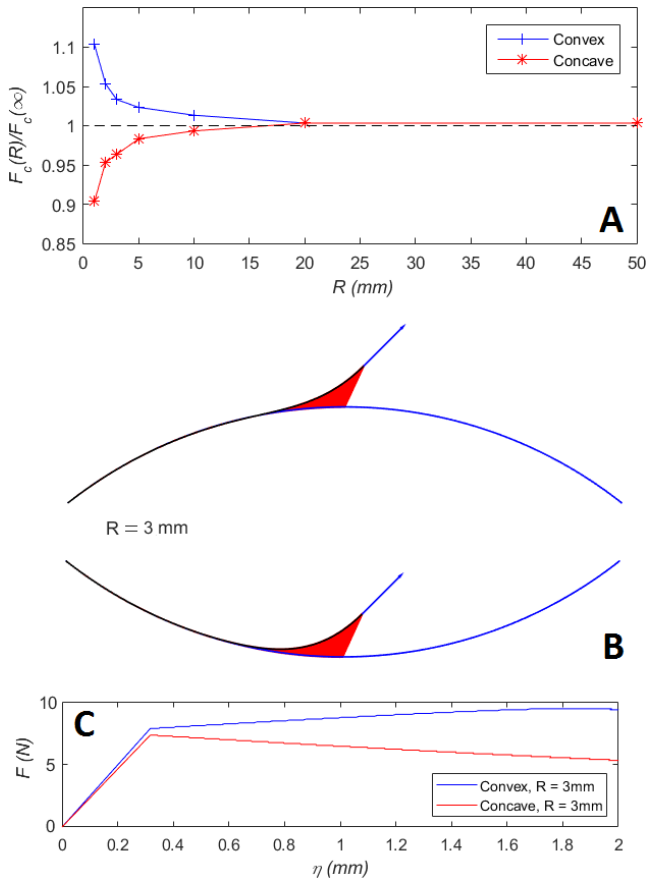

Figure 7. (A) Normalized peeling force as a function of the radius of curvature of the substrate for concave and convex surfaces. (B) Corresponding deformation states. (C) Corresponding force F versus displacement η during peeling test.

value of equation (4) as the substrate becomes stiffer. This increase is the result of two positive mechanisms: first, the distribution of the load in the interface becomes wider, which reduces the load concentration in the vicinity of the peeling line; second, as a result of the substrate deformation, the local peeling angle, i.e. the angle between the applied external load and the deformed surface of the substrate, decreases. This mechanism is also favourable for an increase in the detachment force. A limit of this gain lies in the fact that the attached length of the tape might not be long enough to indefinitely extend the width of the distribution. In this case, the peeling force increase is limited.

Notice that these results are in contrast with the experimental observations in [32], but as the authors themselves point out therein, the measurements are largely affected by other characteristics of the adopted soft substrates, such as surface chemistry, capillary adhesion, friction, etc, all of which are not assumed to vary in our model.

6. Discussion

We have modelled different geometrical and elastic features of the substrate surface profile in order to describe the adhesive behaviour of real materials, where roughness can be observed at different scale levels. We have shown that when the size scale of asperities is small compared to the process zone, their effect on the peeling properties of the tape is limited. We treated this case by considering the roughness as a statistical distribution on the adhesive bond energy to failure, since this implies that the attached length of the film is large with respect to the substrate roughness pattern. We found that the detachment force is close to the one obtained theoretically by taking the average of the distribution. As the size of asperities becomes larger with respect to the attached length of the film, the detached areas become comparable to the process zone, and a decrease in the detachment force is observed. This is consistent with theoretical [17] and experimental [20, 22, 33] data, in which the predicted/measured detachment force for a rough surface is considerably affected by partial bonding, and the pull-off force decreases monotonically with increasing surface roughness. Above a certain roughness size scale, partial bonding is no longer an issue because the tape can conform to the surface pattern. In agreement with theoretical results from [18], there is some variation in the detachment force depending on the type of curved substrate on which the tape must adhere. Simulations show that this is the result of the local perturbation in the process zone due to the change of peeling angle in the zone ahead of the detachment front. As delamination proceeds,

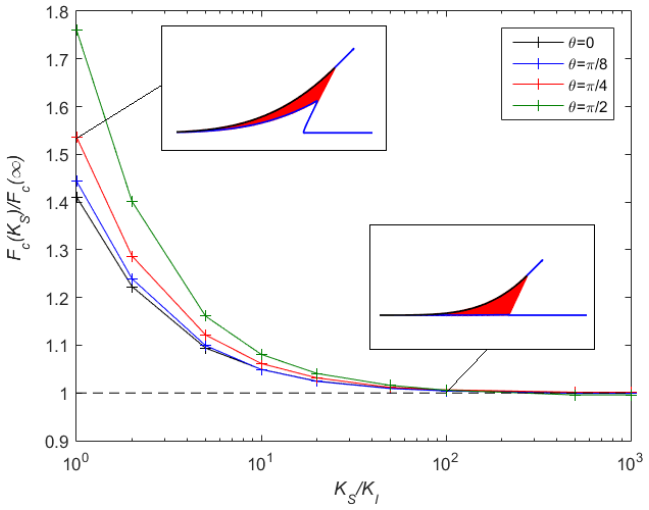

Figure 8. Normalized peeling force as a function of the substrate compliance for various peeling angles. Inset: deformation states for various deformed substrates.

the detachment force is no longer constant; rather, it increases or decreases depending on the criticality of the new distribution emerging from the varying angle of the attached length. The latter observation is consistent with the increase in detachment force obtained experimentally above a certain roughness in [19]. This is because a non-negligible fraction of tape-like contacts is likely to be subjected to a smaller peeling angle as delamination proceeds, and therefore a larger peeling force during simultaneous detachment. All of these results are modified by non-negligible substrate compliance, which we show to be advantageous to adhesive properties in the case of a uniform surface. Further dedicated experimental tests to validate these numerical results would be desirable in the future.

7. Conclusions

In conclusion, we have developed a numerical model to simulate the peeling of adhesive tape-like structures that is focused on the adhesive interface between tape and substrate. The numerical procedure has been validated with a classical thin film peeling theoretical model, and further studies on the interface and substrate properties have been proposed. It has been shown that modelling the interfacial zone where the adhesive bonds are loaded, referred to as the 'process zone', allows us to capture some effects not predicted by the theoretical model, such as imperfect bonding, the geometry of the substrate surface, or substrate deformations within the process zone. The presented model and simulation contribute to a better understanding of the mechanisms and possible optimization of adhesive structures.

Acknowledgments

NMP is supported by the European Commission under the Graphene FET Flagship (WP14 'Polymer composites' No. 604391) and FET Proactive 'Neurofibres' grant No. 732344. FB is supported by 'Neurofibres' grant No. 732344. This work was carried out within the COST Action CA15216 'European Network of Bioadhesion Expertise: Fundamental Knowledge to Inspire Advanced Bonding Technologies'. Computational resources were provided by hpc@polito (www.hpc.polito.it).

Appendix

Further details regarding the implementation of the numerical model are provided below. For the tape elements linking two nodes i and j of the model, mechanical equilibrium is implemented using co-rotational truss formulation [34]. The material and geometric local stiffness matrices are given by the following:

$$\mathbf{K_{Tm}} = \frac{Ebw}{\Delta x}\begin{bmatrix} n_1{}^2 & n_1n_2 & -n_1{}^2 & -n_1n_2 \\ n_1n_2 & n_2{}^2 & -n_1n_1 & -n_2{}^2 \\ -n_1{}^2 & -n_1n_2 & n_1{}^2 & n_1n_2 \\ -n_1n_2 & -n_2{}^2 & n_1n_2 & n_2{}^2 \end{bmatrix}, \tag{A.1}$$

$$\mathbf{K_{Tg}} = \frac{Ebw}{\Delta x}\frac{\delta_T}{\Delta x + \delta_T}\begin{bmatrix} 1 & 0 & -1 & 0 \\ 0 & 1 & 0 & -1 \\ -1 & 0 & 1 & 0 \\ 0 & -1 & 0 & 1 \end{bmatrix}, \tag{A.2}$$

where E is the elastic modulus of a tape element, b is its thickness, w is its width, Δx is its length (corresponding to the discretization length), δ_T is its elongation, and n_1 and n_2 are the components of the (deformed) tape element direction vector in 2D space, i.e.

$$n_1 = \frac{x_j + u_j - x_i - u_i}{\Delta x + \delta_T}, \tag{A.3}$$

$$n_2 = \frac{y_j + v_j - y_i - v_i}{\Delta x + \delta_T}, \tag{A.4}$$

where $\mathbf{x} = \begin{bmatrix} x & y \end{bmatrix}$ is the coordinate vector of a node, and $\mathbf{u} = \begin{bmatrix} u & v \end{bmatrix}$ is its displacement after deformation. Its contribution to the internal force vector is

$$\mathbf{Q_{Ti}} = \frac{Ebw}{\Delta x}\delta_{\mathrm{T}} \begin{bmatrix} n_1 \\ n_2 \\ -n_1 \\ -n_2 \end{bmatrix}. \tag{A.5}$$

On the other hand, the interface bonds act on one node each. For a linear elastic traction–separation law, the contribution of an interface bond to the stiffness matrix is given by

$$\mathbf{K_I} = K_{\mathrm{I}} w \Delta x \begin{bmatrix} 1 & 0 \\ 0 & 1 \end{bmatrix}, \tag{A.6}$$

where k_{I} is the stiffness of an interface bond. Its contribution to the internal force vector thus becomes

$$\mathbf{Q_{Ii}} = K_{\mathrm{I}} w \Delta x \delta_{\mathrm{I}} \begin{bmatrix} u_i \\ v_i \end{bmatrix}. \tag{A.7}$$

The external force vector $\mathbf{Q_e}$ contains the components of the external load acting on the system. Once all contributions are assembled into the linear system, mechanical equilibrium is obtained by updating the nodal displacement according to the following iterative scheme:

$$\mathbf{u} + \left(\mathbf{K_{Tm}} + \mathbf{K_{Tg}} + \mathbf{K_I}\right)^{-1} \left(\mathbf{Q_e} - \mathbf{Q_{Ti}} - \mathbf{Q_{Ii}}\right) \rightarrow \mathbf{u}. \tag{A.8}$$

The two-norm of the residual $\|\mathbf{Q_e} - \mathbf{Q_{Ti}} - \mathbf{Q_{Ii}}\|$ is used as the convergence criterion.

ORCID iDs

Federico Bosia https://orcid.org/0000-0002-2886-4519
Nicola M Pugno https://orcid.org/0000-0003-2136-2396

References

[1] Qiang C and Pugno N M 2013 Bio-mimetic mechanisms of natural hierarchical materials: a review *J. Mech. Behav. Biomed. Mater.* **19** 3–33
[2] Xia F and Jiang L 2008 Bio-inspired, smart, multiscale interfacial materials *Adv. Mater.* **20** 2842–58
[3] Youngblood J P and Sottos N R 2008 Bioinspired materials for self-cleaning and self-healing *MRS Bull.* **33** 732–41
[4] Sanchez C, Arribart H and Giraud Guille M 2005 Biomimetism and bioinspiration as tools for the design of innovative materials and systems *Nat. Mater.* **4** 277–88
[5] Varenberg M, Pugno N M and Gorb S N 2010 Spatulate structures in biological fibrillar adhesion *Soft Matter* **6** 3269–72
[6] Autumn K, Dittmore A, Santos D, Spenko M and Cutkosky M 2006 Frictional adhesion: a new angle on gecko attachment *J. Exp. Biol.* **209** 3569–79
[7] Pesika N S, Tian Y, Zhao B, Rosenberg K, Zeng H, McGuiggan P, Autumn K and Israelachvili J N 2007 Peel-zone model of tape peeling based on the gecko adhesive system *J. Adhes.* **83** 383–401
[8] Tian Y, Pesika N, Zeng H and Israelachvili J 2006 Adhesion and friction in gecko toe attachment and detachment *Proc. Natl. Acad. Sci.* **103** 19320–5
[9] Rivlin R S 1944 The effective work of adhesion *Paint Technol.* **IX** 2611–4
[10] Kendall K 1975 Thin-film peeling-the elastic term *J. Phys. D: Appl. Phys.* **8** 1449
[11] Autumn K 2002 Evidence for van der Waals adhesion in gecko setae *Proc. Natl. Acad. Sci.* **99** 12252–6
[12] Federle W, Riehle M, Curtis A S G and Full R J 2002 An integrative study of insect adhesion: mechanics and wet adhesion of pretarsal pads in ants *Integr. Comparat. Biol.* **42** 1100–6
[13] Zhou Y, Robinson A, Steiner U and Federle W 2014 Insect adhesion on rough surfaces: analysis of adhesive contact of smooth and hairy pads on transparent microstructured substrates *J. R. Soc. Interface* **11** 20140499
[14] Gillies A G, Henry A, Lin H, Ren A, Shiuan K, Fearing R S and Full R J 2014 Gecko toe and lamellar shear adhesion on macroscopic, engineered rough surfaces *J. Exp. Biol.* **217** 283–9
[15] Niewiarowski P H, Stark A Y and Dhinojwala A 2016 Sticking to the story: outstanding challenges in gecko-inspired adhesives *J. Exp. Biol.* **219** 912–9
[16] Persson B 2003 On the mechanism of adhesion in biological systems *J. Chem. Phys.* **118** 7614–21
[17] Persson B N J and Gorb S 2003 The effect of surface roughness on the adhesion of elastic plates with application to biological systems *J. Chem. Phys.* **119** 11437
[18] Peng Z L and Chen S H 2011 Effects of surface roughness and film thickness on the adhesion of a bioinspired nanofilm *Phys. Rev.* E **83** 051915
[19] Huber G, Gorb S, Hosoda N, Spolenak R and Arzt A 2007 Influence of surface roughness on gecko adhesion *Acta Biomater.* **3** 607–10
[20] Cañas N, Kamperman M, Völker B, Kroner E, McMeeking R and Arzt E 2012 Effect of nano- and micro-roughness on adhesion of bioinspired micropatterned surfaces *Acta Biomater.* **8** 282–8
[21] Lin P, Vajpayee S, Jagota A, Hui C and Yang S 2008 Mechanically tunable dry adhesive from wrinkled elastomers *Soft Matter* **4** 1830–5
[22] Jagota A and Hui C 2011 Adhesion, friction, and compliance of bio-mimetic and bio-inspired structured interfaces *Mater. Sci. Eng.* R **72** 253–92
[23] Rivlin R S and Thomas A G 1997 Rupture of rubber. I. Characteristic energy for tearing *Collected Papers of RS Rivlin* (New York: Springer) pp 2615–42
[24] Kaelble D H 1960 Theory and analysis of peel adhesion: bond stresses and distributions *Trans. Soc. Rheol.* **4** 45–73
[25] Pugno N M 2011 The theory of multiple peeling *Int. J. Fract.* **171** 185–93
[26] Cox H L 1952 The elasticity and strength of paper and other fibrous materials *Br. J. Appl. Phys.* **3** 72
[27] Peng Z and Chen S 2015 Effect of bending stiffness on the peeling behavior of an elastic thin film on a rigid substrate *Phys. Rev.* E **91** 042401
[28] Barenblatt G I 1962 The mathematical theory of equilibrium cracks in brittle fracture *Adv. Appl. Mech.* **7** 55–129
[29] Atkinson K 2008 *An Introduction to Numerical Analysis* (New York: Wiley)
[30] Bullock J and Federle W 2009 Division of labour and sex differences between fibrillar, tarsal adhesive pads in beetles: effective elastic modulus and attachment performance *J. Exp. Biol.* **212** 1876–88
[31] Henrik P, Michels J and Gorb S 2013 Evidence for a material gradient in the adhesive tarsal setae of the ladybird beetle *Coccinella septempunctata Nat. Commun.* **4** 1661
[32] Klittich M R, Wilson M, Bernard C, Rodrigo R, Keith A, Niewiarowski P H and Dhinojwala A 2017 Influence of substrate modulus on gecko adhesion *Sci. Rep.* **7** 43647
[33] Fuller K and Tabor D 1975 The effect of surface roughness on the adhesion of elastic solids *Proc. R. Soc.* A **345** 327
[34] Yaw L L 2011 *3D Co-Rotational Truss Formulation* (online) available at: (https://gab.wallawalla.edu/~louie.yaw/Co-rotational_docs/3Dcorot_truss.pdf)